Journal of Materials Chemistry C

Accepted Manuscript

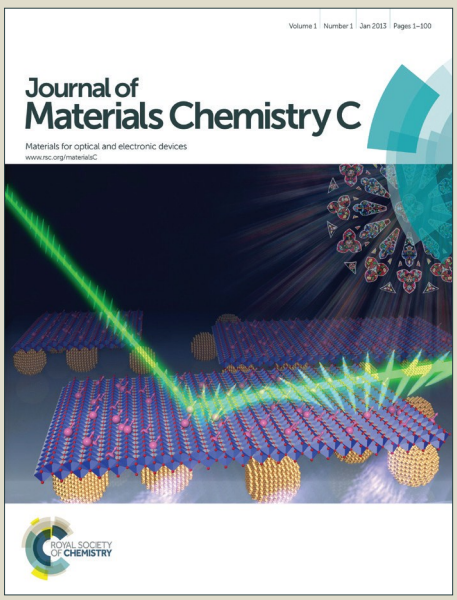

ROYAL SOCIETY OF CHEMISTRY

www.rsc.org/materialsC

Ultrathin Nanosheets of $CrSiTe_3$: A Semiconducting Two-Dimensional Ferromagnetic Material

Ming-Wei Lin[1†], Houlong L. Zhuang[1†], Jiaqiang Yan[2,3], Thomas Zac Ward[3], Alexander A. Puretzky[1], Christopher M. Rouleau[1], Zeng Gai[1], Liangbo Liang[4], Vincent Meunier[4], Bobby Sumpter[1], Panchapakesan Ganesh[1], Paul R. C. Kent[1], David B. Geohegan[1], David G. Mandrus[2,3], Kai Xiao[1*]

[1]Center for Nanophase Materials Sciences, Oak Ridge National Laboratory, Oak Ridge, TN 37831, USA.
[2]Department of Materials Science and Engineering, University of Tennessee, Knoxville, TN 37996, USA.
[3]Materials Science and Technology Division, Oak Ridge National Laboratory, Oak Ridge, TN 37831, USA.
[4]Department of Physics, Applied Physics, and Astronomy, Rensselaer Polytechnic Institute, Troy, New York 12180, USA.
*To whom correspondence should be addressed: E-mail: xiaok@ornl.gov
[†]These authors contributed equally to this work.

Notice: This manuscript has been authored by UT-Battelle, LLC, under Contract No. DE-AC05-00OR22725 with the U.S. Department of Energy. The U.S. Government is authorized to reproduce and distribute reprints for Government purposes notwithstanding any copyright notation hereon. The Department of Energy will provide public access to these results of federally sponsored research in accordance with the DOE Public Access Plan (http://energy.gov/downloads/doe-public-access-plan).

Abstract

Finite range ferromagnetism and antiferromagnetism in two-dimensional (2D) systems within an isotropic Heisenberg model at non-zero temperature were originally proposed to be impossible. However, recent theoretical studies using an Ising model have recently shown that 2D magnetic crystals can exhibit magnetism. Experimental verification of existing 2D magnetic crystals in this system has remained exploratory. In this work we exfoliate the $CrSiTe_3$, a bulk ferromagnetic semiconductor, to mono- and few-layer 2D crystals onto a Si/SiO_2 substrate. The Raman spectra show the good stability and high quality of the exfoliated flakes, consistent with the computed phonon spectra of 2D $CrSiTe_3$, giving a strong evidence for the existence of 2D $CrSiTe_3$ crystals. When the thickness of the $CrSiTe_3$ crystals is reduced to few-layers, we observed a clear change in resistivity at 80~120 K, consistent with the theoretical calculations on the Curie temperature (T_c) of ~80 K for the magnetic ordering of 2D $CrSiTe_3$ crystals. The ferromagnetic mono- and few-layer 2D $CrSiTe_3$ indicated here should enable numerous applications in nano-spintronics.

KEYWORDS: $CrSiTe_3$, ferromagnetism, field-effect transistor, Curie temperature

Introduction

The emergence of novel properties and potential applications of two-dimensional (2D) crystals has recently stimulated considerable worldwide attention[1-3]. A particularly interesting class of candidate 2D crystals is the layered magnetic semiconductors which can simultaneously display semiconductor characteristics and magnetic ordering that are advantageous for optoelectronics and nano-spintronics applications.[4-6] Both ferromagnetic (FM) and antiferromagnetic (AFM) layered semiconductors have been characterized in bulk form, including their crystallographic and magnetic structures.[7-11] For example, chromium tellurosilicate ($CrSiTe_3$) is a FM layered transition-metal chalcogenide (TMD) semiconductor, and exhibits ferromagnetic ordering at 32 K in the bulk.[7-8] Heisenberg type ferromagnetism has been found below 6.25 K for K_2CuF_4 bulk crystals due to one percent of the anisotropic interlayer exchange interaction.[11] Unlike other non-magnetic 2D layered materials that require edge,[12, 13] strain engineering[14,15], a balanced hole-electron "resonance" condition,[16] or so called phase incorporation due to vacancies[17] to achieve magnetic properties, the magnetic ordering in these 2D systems, such as $CrSiTe_3$ or K_2CuF_4, could inherit from their parent layered 3D system. However, the existence of 2D magnetic ordering is unclear, particularly whether this is inherited from the parent 3D system. In an earlier report, calculations by Mermin and Wagner predicted that spontaneous ferromagnetism and anti-ferromagnetism should not exist based on a 2D isotropic Heisenberg model with long-range order at non-zero temperature.[18] Bruno also proved the absence of spontaneous magnetic ordering in one- or two-dimensional Heisenberg systems with long-range interactions at finite temperatures.[19] Recently, the possibility of 2D K_2CuF_4 crystals to form free-standing 2D flakes by exfoliation with a robust magnetic moment of a Kosterlitz-Thouless type system was predicted from a first-principles theoretical analysis.[5]

Experimentally, a 2D Mn stearate ($MnSt_2$) magnet has been demonstrated by deposition on a Si substrate using Langmuir-Blodgett technique.[20] Moreover, a magnetic phase transition exhibiting a thickness dependence due to a dramatic critical exponent β change has been reported for Ni thin film[21-22], indicating changes in magnetic ordering for a 2D Ising system at non-zero temperature. Recent studies associated with TMDs (TiCoO, CoSe and ZnO) nanosheets using chemical solution approaches also showed the semiconductor characteristics with magnetism,[23-26] demonstrating the existence of magnetism for 2D nanosheets at non-zero temperatures. To resolve the debate on the presence and origin of magnetism in these systems, layered 2D semiconductors, such as $CrSiTe_3$, can be exfoliated layer-by-layer from a bulk crystal and can be used as excellent testbeds.

$CrSiTe_3$ is an indirect layered semiconductor with indirect and direct band gaps at 0.4 eV and 1.2 eV, respectively.[8] As shown in Figure 1, $CrSiTe_3$ is a layered material formed from stacks of Te-(Cr, Si)-Te sandwich layers. One layer is composed of a Si_2Te_6 with two Cr ions inserted between two layers of Te planes, leading to a van der Waals gap.[27] Bulk $CrSiTe_3$ exhibits a quasi-2D Ising ferromagnetic behavior at T_c = 33 K [28, 29] Our previous report shows the strong coupling between the magnetic and lattice degrees of freedom by the measurements of the phonons across the 33K ferromagnetic transition.[8] The Si-Te stretching and Te displacement modes are sensitive to the magnetic ordering transition,[8] which indicates the magnetic ordering transition could be modified by a phonon dimensionality crossover in 2D systems due to the quantum confinement of phonons. Recently, it has been predicted that there existed the dynamic stability of 2D $CrSiTe_3$ with ferromagnetic ordering based on Heisenberg model and the Curie temperature (T_c) would be dramatically shifted to higher temperature in single layer compared to the bulk.[30,31] In some published results, they also showed the existence of uniaxial easy axis for

monolayer $CrSiTe_3$ crystal based on 2D Ising model, which was more suitable to predict the T_c change.[6,32] However, other theoretical calculations predict that monolayer $CrSiTe_3$ should be antiferromagnetic with a zigzag spin texture when the significance of second and third order exchange interactions are considered.[6] Although theoretical studies have predicted the existence of such a 2D magnetic semiconductor, experimental confirmation is still lacking. Unlike graphene or binary semiconductors such as $MoSe_2$, and GaSe, which have been synthesized using chemical vapor deposition (CVD) and vapor phase deposition (VPD),[33, 34] the monolayer and few-layer of 2D $CrSiTe_3$ crystals are much harder to synthesize. Recent advances in micro-exfoliation techniques have made it possible to produce 2D magnetic single crystals that were previously inaccessible to the community.[35, 36]

In this work, single-crystalline monolayer and few-layer $CrSiTe_3$ crystals were prepared from the bulk crystals by a simple mechanical exfoliation method. The Raman spectra show the good stability and high quality of the exfoliated flakes, consistent with the computed phonon spectra of 2D $CrSiTe_3$, giving a strong evidence for the existence of 2D $CrSiTe_3$ crystals. When the thickness of the $CrSiTe_3$ crystals is reduced to few-layers, we observed a clear change in resistivity at 80~120 K, which strongly supports the theoretically predicted temperature enhancement of magnetic ordering (T_c ~80 K) for a 2D $CrSiTe_3$ crystals. This study, indicating a combination of semiconducting and magnetic characteristics of 2D $CrSiTe_3$, appears promising for a new class of 2D materials for nano-spintronic applications.

Experimental and theoretical methods

$CrSiTe_3$ flakes were first deposited by a mechanical cleavage method onto 290-nm-thick, heavily doped Si/SiO_2 substrates. Sample thicknesses were characterized by both a Nikon LV150 optical microscope (OM) and an atomic force microscope (AFM) (Bruker Dimension Icon).

MicroRaman spectroscopy (Renishaw, 532 nm excitation with a 50x objective) was performed to characterize the typical Raman modes of $CrSiTe_3$ flakes for different thickness. $CrSiTe_3$ FET devices were fabricated using standard e-beam lithography (FEI Nanolab 600 dual beam), followed by metal deposition using an e-beam evaporator with a layer of 5 nm Ti and 30 nm Au for both source and drain electrodes. The electrical properties of the devices were then measured in a cryogenic vacuum chamber (Desert Cryogenics, ~10^{-6} torr) with a Keithley 4200 semiconductor analyzer in a back-gating configuration.

Electronic structure calculations of monolayer $CrSiTe_3$ were carried out using the projector augmented wave (PAW) method within density functional theory (DFT) as implemented in the plane wave code VASP.[37, 38] The cutoff energy of the plane-wave basis was set to 700 eV. To represent the localized Cr *d* orbitals the local density functional approximation (LDA) combined with an on-site Hubbard *U* were empolyed.[39] In the main text, results obtained using U_{eff} = 3.5 eV are primarily reported. This U_{eff} parameter has been shown to reproduce reasonable spin-up/down bandgaps of bulk $CrSiTe_3$. Results using various U_{eff} ranging from 0 to 10 eV are given in the supporting materials Figure S1. The Monkhorst-Pack scheme was sued for and *k*-point sampling employing a 9 x 9 x 1 Γ-centered grid.

Calculations were also performed to predict the non-resonant Raman scattering spectra of $CrSiTe_3$ using fully relaxed geometries. Since the Raman scattering intensity *I* is proportional to $|e_{\mathrm{i}} \cdot \tilde{R} \cdot e_{\mathrm{s}}|^2$, the calculations of the Raman tensors $\tilde{R}$ are most important. This requires information on the phonon frequencies, phonon eigenvectors and the changes of the dielectric constant tensors by phonon vibrations.[40] To calculate Raman scattering intensities, calculation of the dynamic matrix and derivatives of the dielectric constant tensors are required. The dynamic matrix was calculated using the *ab initio* direct method[41] as implemented in the PHONON

software.[42] In this finite difference scheme, the Hellmann-Feynman forces in the supercell were computed by VASP for both positive and negative atomic displacements (δ = 0.03 Å) and used in PHONON to construct the dynamic matrix. Diagonalization of the dynamic matrix provides phonon frequencies and eigenvectors. For both positive and negative atomic displacements (δ = 0.03 Å) in the single unit cell, the dielectric tensors were computed by VASP using density functional perturbation theory and then imported into PHONON to generate their derivatives. From this, the Raman intensity for every phonon mode was obtained for a given laser polarization and wavelength to yield a Raman spectrum after Gaussian broadening.

Results and discussion

$CrSiTe_3$ single crystals were grown using a self-flux technique as shown our previous work.[8] The as-grown crystals are plate-like and thickness is around 5 mm. The crystals exhibited very high purity and excellent crystallinity. The van der Waals interaction in the layered $CrSiTe_3$ single crystals allows it to be thinned down to atomically thin 2D crystals using mechanic exfoliation. The cleavage energy of $CrSiTe_3$ (43.7 meV/atom) computed from density-functional theory (DFT) calculations is significantly smaller than that of MoS_2 (77 meV/atom). Thus, $CrSiTe_3$ layers of ~3-5 nm in thickness can be easily produced from exfoliation using adhesive tape, and even flakes as thin as only single layer (0.8 nm) are accessible, as illustrated by the image of a large (>5 μm) single layer flake in Figure 2. Figure 2 (c) and (d) show thickness of 0.8 nm and 3 nm (insets shown the line profiles) corresponding to exposed regions of mono- and four-layer flakes, respectively. These results establish that a monolayer of CST on Si/SiO_2 substrate can be made.

The quality and stability of the atomically thin $CrSiTe_3$ single crystal flakes were further characterized by Raman spectroscopy and calculations of the phonon spectrum for monolayer of

$CrSiTe_3$ crystals. Figure 3(a) shows the Raman spectrum of $CrSiTe_3$ flakes with various thicknesses ranging from monolayer to bulk. We observed three peaks located at 101 cm^{-1}, 125 cm^{-1} and 142 cm^{-1}, which can be assigned to E_g and A^2_g and A^1_g modes, respectively. According to our calculations these modes correspond to in-plane and out-of-plane vibrations of Te atoms (see Fig. 3(b)). The detailed simulation results for the Raman active modes in a $CrSiTe_3$ crystal are shown in Figure S2. The calculated frequencies agree well with the measured positions of the Raman peaks. In addition, all phonon frequencies observed in the first Brillouin zone are real, confirming the dynamic stability of a single $CrSiTe_3$ layer. The observed peaks show a few wavenumbers blue shift as the number of layers decreases that can be related to variations of phonon spectra due to the reduced dimensionality.[34] We also observe the dramatic change in Raman spectra when the thickness decreases from 7 nm to 3 nm, i.e., all three sharp peaks disappear and only a broad feature at ~160 cm^{-1} still remains in the spectra, but with much lower intensity. We also observe the dramatic change of Raman spectra starting at 7 nm thickness. The possible reason is that the spin ordering is changed along the sample thinning. The spin-lattice coupling is noticeable in $CrSiTe_3$ and different spin states could lead to different lattice constants,[8] thus induce to different phonon frequencies. Further spin study is needed and underway.

We have fabricated 2D $CrSiTe_3$ field-effect transistor (FET) devices using standard electron-beam lithography. Figure 4(a) depicts a schematic diagram of the 2D $CrSiTe_3$ FET device on a Si/SiO_2 substrate with source/drain electrodes. The optical micrograph also demonstrates a clear image of the 2D $CrSiTe_3$ FET device shown in Figure 4(b). Although we are able to thin $CrSiTe_3$ crystals down to single layer, successful devices with good electrical contacts can be prepared only on flakes with thickness ≥ 7 nm. Based on the measurement of

output curves shown in Figure 4(c) in a back-gating configuration, these $CrSiTe_3$ FET devices display p-type semiconductor characteristics. The linear output curves indicate nearly Ohmic contacts at 295 K and 6 K. Figure 4(d) shows the I_{ds}-V_{bg} transfer curves measured on a 7 nm thick $CrSiTe_3$ device at different temperatures down to 6 K with V_{ds} = 1 V. The inset in Figure 4 (d) shows the mobility are increased as the temperature increasing, demonstrating the same trend as found in single layer of MoS_2 in the same gating configuration.[43] The mobility (~0.01 cm^2/Vs at T = 295 K) was calculated using the equation $\mu = \frac{1}{Cox}\left(\frac{L}{WVds}\right)\left(\frac{dI}{dVbg}\right)$ extracted from the linear region of transport curves I_{ds}-V_{bg}, where L is the channel length, W is the channel width, V_{ds} = 1 V and C_{ox} = 1.2x10^{-8} F/cm^2 is the capacitance between channel and the back gate per unit area ($C_{ox} = \varepsilon_0\varepsilon_r/d_{ox}$, ε_0 = 8.85x10^{-12} F/m, ε_r = 3.9 and d_{ox} = 290 nm).

The electronic band structure of monolayer $CrSiTe_3$ was calculated from first-principles calculations using density-functional theory (DFT). Figure 5(a) shows the spin-polarized electronic band structures of monolayer $CrSiTe_3$, confirming an indirect bandgap semiconductor behavior of monolayer $CrSiTe_3$. The bandgaps of FM ordering as a function of U_{eff} are presented in Figure S1 (c). The gap sizes for spin-up and spin-down states are 0.57 eV and 0.65 eV, respectively. For bulk $CrSiTe_3$, using the same U_{eff} the calculated spin-up and spin-down bandgaps are 0.39 eV and 0.65 eV, respectively. The enhanced spin-up bandgap of monolayer $CrSiTe_3$ compared to that of the bulk is due to quantum confinement, which is an intrinsic property at low dimensionality and similar to other 2D semiconductors.[44, 45] Furthermore, Figure 5(b) shows the density of states of monolayer $CrSiTe_3$, which illustrates that the Cr *d* and Te *p* orbitals are involved in superexchange interactions between the spins of neighboring Cr^{3+} ions.

Table 1 provides a comparison between FM and AFM structure, magnetic moment and formation energy as determined by first-principles calculations for monolayer $CrSiTe_3$. As can

be seen, the lattice constants of monolayer $CrSiTe_3$ with both FM (6.69 Å) and AFM (6.66 Å) orderings are similar, as are their magnetic moments. The calculated magnetic moments are 3.0 μ_B for both magnetic orderings. This value is the same as the spin magnetic moment of an isolated Cr^{3+} ion, implying that the orbital magnetic moments are largely quenched in monolayer $CrSiTe_3$. Indeed, turning on spin-orbit coupling (SOC) in the calculation yields a similar total magnetic moment, which indicates a weak SOC. The ground state energy of monolayer $CrSiTe_3$ was calculated for both FM and AFM orderings. The possible antiferromagnetic spin textures, Néel, stripy, and zigzag configurations, have been considered and computed (see Figure S4). Furthermore, we calculated the first, second, and third nearest-neighboring exchange constants with the computation details described in the supplemental material and determined J_1, J_2, and J_3 as -2.39 meV, 0.00 meV, and +0.18 meV, respectively. This suggests that the dominant exchange coupling comes from the first nearest-neighboring Cr-Cr pair interactions. Therefore, the energy of FM monolayer $CrSiTe_3$ is smaller than the AFM one, showing that the ground-state monolayer $CrSiTe_3$ exhibits ferromagnetic ordering. In addition, we carried out similar calculations of exchange coupling constants for p-type doped single-layer $CrSiTe_3$ by using a 2×2 supercell model with 0.155 electrons removed from the same supercell of pristine single-layer $CrSiTe_3$ with 288 electrons. This is equivalent of *p*-type doping with a very high hole concentration of 10^{13} cm^{-2}. From Figure S4 (f), we can see that the FM structure is still the ground state. Following the same procedure, we obtain the exchange coupling parameters of -2.39 meV, 0.02 meV, and +0.18 meV, which are nearly identical to those in the undoped case. This suggests that *p*-type doping almost has no effects on the Curie temperature.

Another important characteristic of the 2D $CrSiTe_3$ material is ferromagnetism perseverance in low dimensionality with changing Curie temperature T_c. The T_c change has been reported in other multilayered systems from 3D to 2D.[21,22,46,47] From our theoretical calculations

using a 2D Ising model, T_c can reach values up to ~80 K for monolayer $CrSiTe_3$ with magnetic moment $3\mu_B$ as shown in Figure 6 (a). The inset of Figure 6 (a) shows the susceptibility as a function of temperature for monolayer $CrSiTe_3$. The higher T_c in monolayer $CrSiTe_3$ can be understood as possibly resulting from the competition between interlayer and intralayer exchange interactions compared with bulk. The exchange coupling interaction becomes dominated by intralayer Cr-Cr superexchange mediated by Te ions as one proceeds toward a monolayer of $CrSiTe_3$, which gives higher in-plane interaction energy associated with higher T_c. Theoretical calculations also indicate higher energy for exchange coupling resulting from intralayer *versus* interlayer interactions. The resistivity measured for 2D $CrSiTe_3$ devices of thicknesses 7 nm shown in Figure 6 (b) is seen to increase exponentially with decreasing temperature in the high temperature regime but then clearly deviate from this behavior starting at 140 K. We found that the resistivities measured between 100-140 K significantly deviated from the average value below 100 K (shown by the dashed line in Fig. 6(b)) which we attribute to the instrumental resolution. Very similar resistivity *versus* temperature was measured for devices with thicknesses of 8.5 nm and 20 nm (shown in Fig. S3). Altogether, the devices showed transitions from the expected exponential increase in resistivity with decreasing temperature, with clear and measurable deviations from this behavior at temperatures ranging between 80~120 K (shown by arrows in Figure S3). Some published results on metal thin film systems have shown that the critical temperature of a FM to AFM phase transition is accompanied by an abrupt change in resistivity at that temperature due to possible scattering caused by change of magnetic moments,[48,49] In our data, the abrupt transition temperature for the resistivity is generally found to decrease with decreasing number of layers, which we believe is likely due to changes in magnetic ordering with reducing dimensionality. This explanation relies upon the

plausible existence of AFM or FM ordering in 2D magnetic semiconductors down to very thin layers. However, absolute proof of the magnetization of monolayer $CrSiTe_3$ by SQUID measurements is currently extremely complicated due to a very weak signal and the difficulty in preparing the uniform 2D flakes using mechanical exfoliation. Such measurements will be the subject of future studies.

Conclusions:

In conclusion, monolayer and few-layers samples of 2D FM $CrSiTe_3$ crystals were isolated after exfoliation and characterized by Raman spectroscopy, allowing the identification of the Raman-active modes predicted from the calculated phonon spectra and confirming the theoretical predictions that monolayer $CrSiTe_3$ is dynamically stable. The exfoliated few-layer samples retained the p-type semiconductor characteristics of bulk $CrSiTe_3$, as characterized by FET devices fabricated from the lithographically-addressed 2D crystals. Ising model calculations predicted an elevated Curie temperature ($T_c \sim 80$ K) for the magnetic ordering of monolayer 2D $CrSiTe_3$ crystals, significantly increased from the bulk ($T_c \sim 33$ K). Consistent with these predictions, temperature-dependent resistivity measurements for the few-layer 2D $CrSiTe_3$ FET devices indicate a clear change in resistivity at elevated temperatures of 80~120 K. These results indicate that ferromagnetic mono- and few-layer 2D $CrSiTe_3$ crystals are promising ultrathin nanomaterials for potential applications in spintronics.

Acknowledgements

Device fabrications supported by the Laboratory Directed Research and Development program (LDRD) project and Raman measurement was conducted at Center for Nanophase Materials Sciences, which is sponsored at Oak Ridge National Laboratory by the Scientific User Facilities Division, Office of Basic Energy Sciences, U.S. Department of Energy. DGM and JQY

acknowledge support from the National Science Foundation under Grant No. NSF DMR-1410428. TZW acknowledge support from the US Department of Energy (DOE), Office of Basic Energy Sciences (BES), Materials Sciences and Engineering Division for PPMS measurements. HZ, PG, PRCK acknowledge support from LDRD project for theoretical calculations.

Electronic Supplementary Information (ESI) Available: Results of theoretical calculations using various U_{eff} ranging from 0 to 10 eV are given in the Figure S1. Detail information of Raman calculations for both monolayer and bulk is shown in the Figure S2. Resistivity *versus* temperature measurements for the thickness of 8.5 nm, 20 nm, 36 nm and 125 nm are demonstrated in the Figure S3. Figure S4 illustrates the energies computed from different AFM spin textures, with p-type doping consideration. See DOI: 10.1039/x0xx00000x

Notes and references

1 Q. H. Wang, K. Kalantar-Zadeh, A. Kis, J. N. Coleman and M.S. Strano, *Nat. Nanotechnol.*, 2012, **7**, 699-712.

2 A. K. Geim and I. V. Grigorieva, *Nature*, 2013, **499**, 419-425.

3 V. Nicolosi, M. Chhowalla, M. G. Kanatzidis, M. S. Strano and J. N. Coleman, *Science*, 2013, **340**, 1226419.

4 S. Lebègue, T. Björkman, M. Klintenberg, R. Nieminen and O. Eriksson, *Physical Review X*, 2013, **3**, 031002.

5 B. Sachs, T. O. Wehling, K. S. Novoselov, A. I. Lichtenstein and M. I. Katsnelson, *Physical Review B*, 2013, **88**, 201402.

6 N. Sivadas, M. W. Daniels, R. H. Swendsen, S. Okamoto and D. Xiao, *Phys. Rev. B*, 2015, **91**, 235425.

7 V. Carteaux, G. Ouvrard, J. C. Grenier and Y. Laligant, *Journal of Magnetism and Magnetic Materials*, 1991, **94**, 127-133.

8 L. D. Casto, A. J. Clune, M. O. Yokosuk, J. L. Musfeldt, T. J. Williams, H. L. Zhuang, M.-W. Lin, K. Xiao, R. G. Hennig, B. C. Sales, J. -Q. Yan and D. Mandrus, *APL Materials*, 2015, **3**, 041515.

9 H. Kabbour, R. David, A. Pautrat, H. -J. Koo, M. -H. Whangbo, G. André and O. Mentré, *Angewandte Chemie International Edition*, 2012, **51**, 11745-11749.

10 M. A. McGuire, H. Dixit, V. R. Cooper and B. C. Sales, *Chemistry of Materials*, 2015, **27**, 612-620.

11 I. Yamada, *Journal of the Physical Society of Japan*, 1972, **33**, 979-988.

12 S. Tongay, S. S. Varnoosfaderani, B. R. Appleton, J. Wu and A. F. Hebard, *Applied Physics Letters*, 2012, **101**, 123105.

13 Z. Zhang, X. Zou, V. H. Crespi and B. I. Yakobson, *ACS Nano*, 2013, **7**, 10475-10481.

14 H. Pan and Y. -W. Zhang, *The Journal of Physical Chemistry C*, 2012, **116**, 11752-11757.

15 S. Yang, C. Wang, H. Sahin, H. Chen, Y. Li, S. -S. Li, A. Suslu, F. M. Peeters, Q. Liu, J. Li and S. Tongay, *Nano Letters*, 2015, **15**, 1660-1666.

16 M. N. Ali, J. Xiong, S. Flynn, J. Tao, Q. D. Gibson, L. M. Schoop, T. Liang, N. Haldolaarachchige, M. Hirschberger, N. P. Ong and R. J. Cava, *Nature*, 2014, **514**, 205-208.

17 L. Cai, J. He, Q. Liu, T. Yao, L. Chen, W. Yan, F. Hu, Y. Jiang, Y. Zhao, T. Hu, Z. Sun and S. Wei, *Journal of the American Chemical Society*, 2015, **137**, 2622-2627.

18 N. Mermin and H. Wagner, *Physical Review Letters*, 1966, **17**, 1133-1136.

19 P. Bruno, *Physical Review Letters*, 2001, **87**, 137203.

20 M. Pomerantz, *Surface Science*, 1984, **142**, 556-570.

21 Y. Li and K. Baberschke, *Physical Review Letters*, 1992, **68**, 1208-1211.

22 M. A. Medvedeva and P. V. Prudnikov, *Journal of Physics: Conference Series*, 2014, **510**, 012024.

23 M. Osada, Y. Ebina, K. Fukuda, K. Ono, K. Takada, K. Yamaura, E. Takayama-Muromachi and T. Sasaki, *Physical Review B*, 2006, **73**, 153301.

24 X. Zhang, J. Zhang, J. Zhao, B. Pan, M. Kong, J. Chen and Y. Xie, *Journal of the American Chemical Society*, 2012, **134**, 11908-11911.

25 T. Taniguchi, K. Yamaguchi, A. Shigeta, Y. Matsuda, S. Hayami, T. Shimizu, T. Matsui, T. Yamazaki, A. Funatstu, Y. Makinose, N. Matsushita, M. Koinuma and Y. Matsumoto, *Advanced Functional Materials*, 2013, **23**, 3140-3145.

26 M. Osada, S. Yoguchi, M. Itose, B. -W. Li, Y. Ebina, K. Fukuda, Y. Kotani, K. Ono, S. Ueda and T. Sasaki, *Nanoscale*, 2014, **6**, 14227-14236.

27 G. Ouvrard, E. Sandre and R. Brec, *Journal of Solid State Chemistry*, 1988, **73**, 27-32.

28 V. Carteaux, F. Moussa and M. Spiesser, *EPL (Europhysics Letters)*, 1995, **29**, 251-256.

29 T. J. Williams, A. A. Aczel, M. D. Lumsden, S. E. Nagler, M. B. Stone, J. –Q. Yan and D. Mandrus, *arXiv* 2015: 1503.08199v1.

30 X. Li and J. Yang, *Journal of Materials Chemistry C*, 2014, **2**, 7071-7076.

31 X. Chen, J. Qi and D. Shi, *Physics Letters A*, 2015, **379**, 60-63.

32 H. L. Zhuang, Y. Xie, P. R. C. Kent and P. Ganesh, *Phys. Rev. B*, 2015, **92**, 035407.

33 X. Wang, Y. Gong, G. Shi, W. L. Chow, K. Keyshar, G. Ye, R. Vajtai, J. Lou, Z. Liu, E. Ringe, B. K. Tay and P. M. Ajayan, *ACS Nano*, 2014, **8**, 5125-5131.

34 X. Li, M. -W. Lin, A. A. Puretzky, J. C. Idrobo, C. Ma, M. Chi, M. Yoon, C. M. Rouleau, I. I. Kravchenko, D. B. Geohegan and K. Xiao, *Sci. Rep.*, 2014, **4**.

35 K. S. Novoselov, A. K. Geim, S. V. Morozov, D. Jiang, Y. Zhang, S. V. Dubonos, I. V. Grigorieva and A. A. Firsov, *Science*, 2004, **306**, 666-669.

36 X. Li, X. Wu and J. Yang, *Journal of the American Chemical Society*, 2014, **136**, 11065-11069.

37 G. Kresse and J. Furthmüller, *Computational Materials Science*, 1996, **6**, 15-50.

38 G. Kresse and D. Joubert, *Physical Review B*, 1999, **59**, 1758-1775.

39 A. I. Liechtenstein, V. I. Anisimov and J. Zaanen, *Physical Review B*, 1995, **52**, R5467-R5470.

40 L. Liang and V. Meunier, *Nanoscale*, 2014, **6**, 5394-5401.

41 K. Parlinski, Z. Q. Li and Y. Kawazoe, *Physical Review Letters*, 1997, **78**, 4063-4066.

42 K. Parlinski, *Computer Code PHONON*, 2010, Krakow, Poland.

43 B. Radisavljevic and A. Kis, *Nat. Mater.*, 2013, **12**, 815-820.

44 G. W. Mudd, S. A. Svatek, T. Ren, A. Patanè, O. Makarovsky, L. Eaves, P. H. Beton, Z. D. Kovalyuk, G. V. Lashkarev, Z. R. Kudrynskyi and A. I. Dmitriev, *Advanced Materials*, 2013, **25**, 5714-5718.

45 Y. Yoon, K. Ganapathi and S. Salahuddin, *Nano Letters*, 2011, **11**, 3768-3773.

46 A. Du and G. Wei, *Australian Journal of Physics*, 1993, **46**, 571-582.

47 L. Capriotti, R. Vaia, A. Cuccoli and V. Tognetti, *Physical Review B*, 1998, **58**, 273-281.

48 J. S. Kouvel and C. C. Hartelius, *Journal of Applied Physics*, 1962, **33**, 1343-1344.

49 M. A. d. Vries, M. Loving, A. P. Mihai, L. H. Lewis, D. Heiman and C. H. Marrows, *New Journal of Physics*, 2013, **15**, 013008.

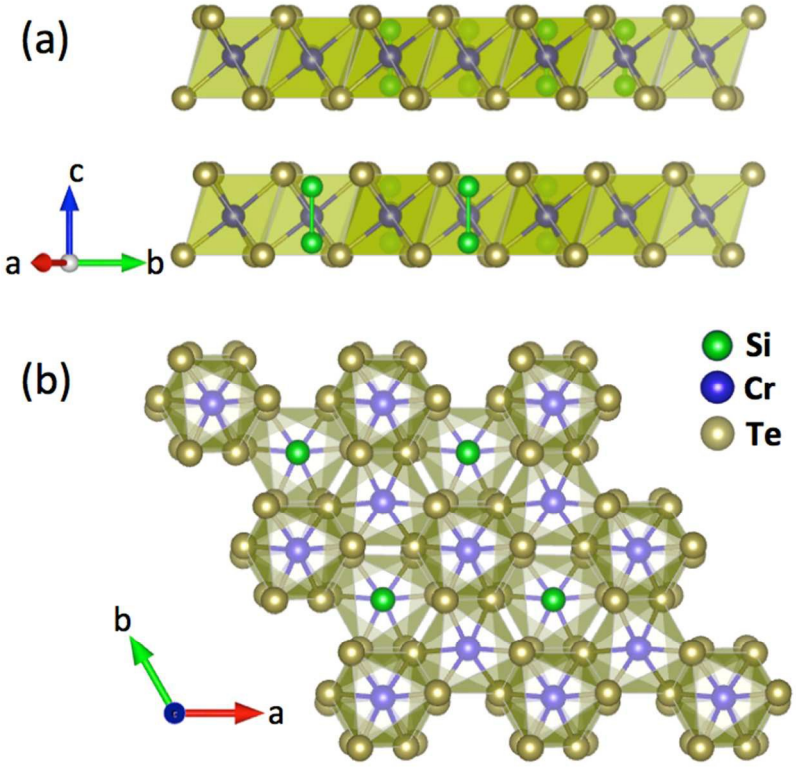

Figure 1. Side (a) and top (b) views of the atomic structure for 2D $CrSiTe_3$.

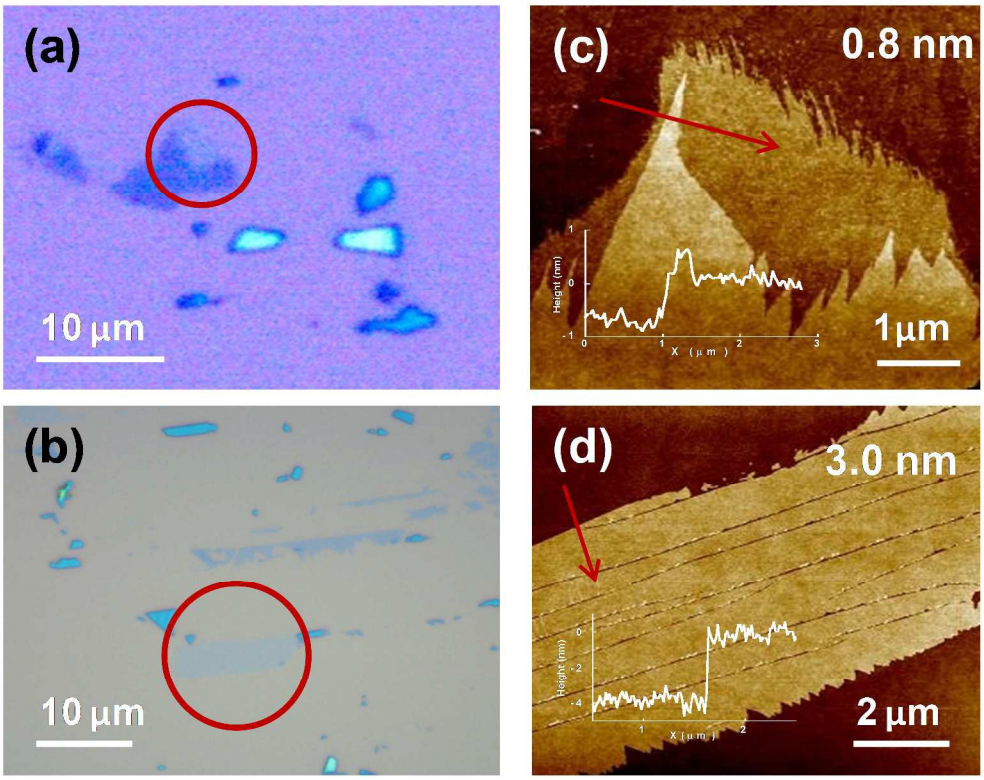

Figure 2. The optical and AFM images of exfoliated 2D $CrSiTe_3$ flakes on Si/SiO_2 substrates. (a) and (b) are optical images showing $CrSiTe_3$ flakes by exfoliation method on Si/SiO_2 substrate with mono and few layers. (c) and (d) are AFM images demonstrating the mono and few-layer $CrSiTe_3$ flakes with respect to (a) and (b). Insets in (c) and (d) are line scan profiles of red arrows.

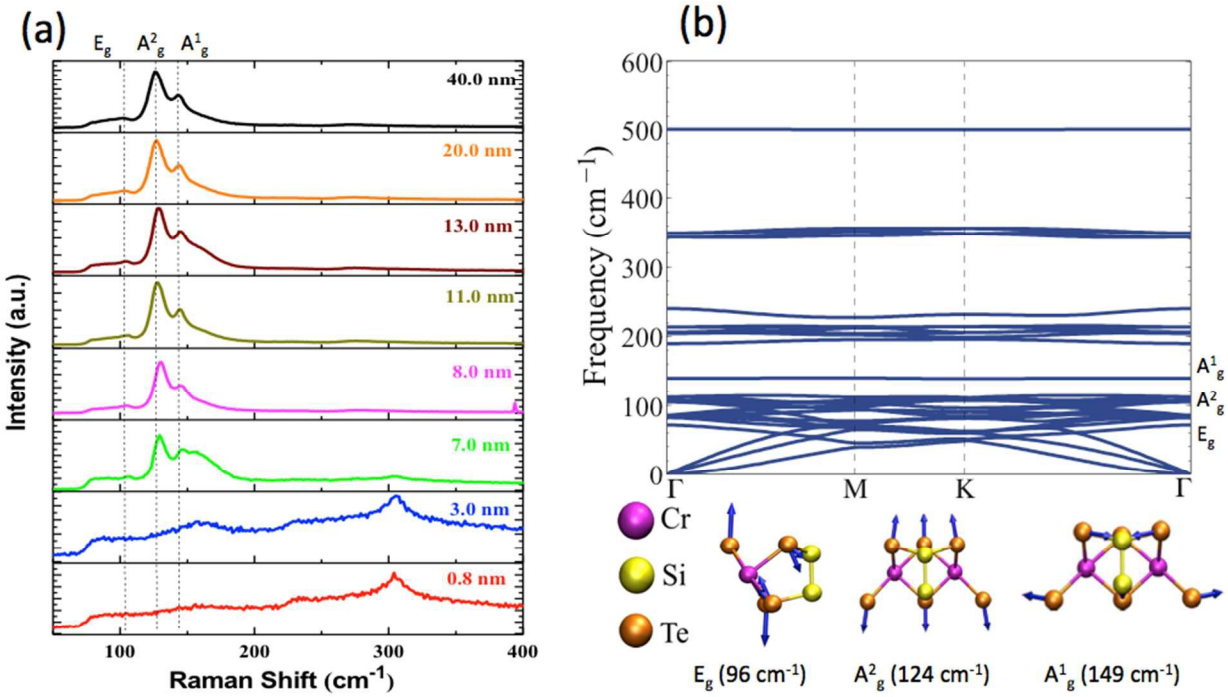

Figure 3. Measured Raman and phonon dispersion spectrum from first principles simulations for $CrSiTe_3$ flakes. (a) illustrates Raman spectrum of $CrSiTe_3$ flakes with different thickness, showing the typical peaks at 142 cm^{-1}, 125 cm^{-1} and 101 cm^{-1}. The broad peak at 304 cm^{-1} belongs to Si. (b) The phonon spectrum demonstrates the dynamic stablity for mono-layer $CrSiTe_3$. The active Raman modes from simulation corresponding to A^1_g (in-plane), A^2_g (out-of-plane) and E_g (out-of-plane) of Te vibrations match the Raman peaks in spectrum from measurement.

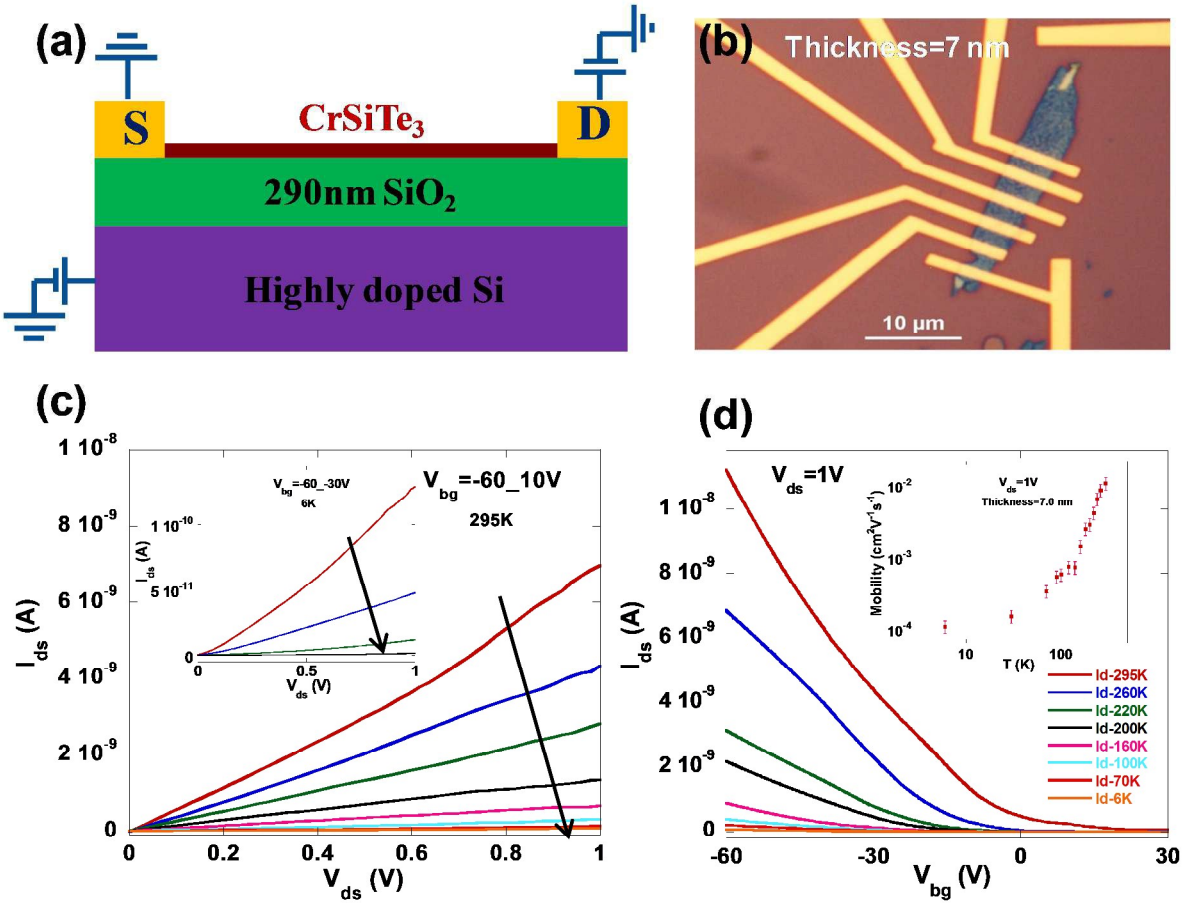

Figure 4. The schematic diagram, optical micrograph and characteristics of $CrSiTe_3$ FET device. (a) The schematic sketch of $CrSiTe_3$ FET device on Si/SiO_2 substrate shows the source/drain electrodes with a layer of Ti 5 nm and Au 30 nm. (b) The OM image shows the top view of $CrSiTe_3$ FET devices with electrodes. (c) I_{ds}–V_{ds} output curves demonstrate linear dependence, giving the nearly ohmic contact of $CrSiTe_3$ FET device at 295 K. Inset is the I_{ds}–V_{ds} curves at 6 K. (d) The transfer curve shows the p-type semiconductor of $CrSiTe_3$ device of 7-nm-thick flake with temperature dependence down to 6 K. The mobility as a function of temperature for $CrSiTe_3$ FET device with thickness of 7.0 nm is shown in the inset, indicating the mobility decreases as decreasing temperature.

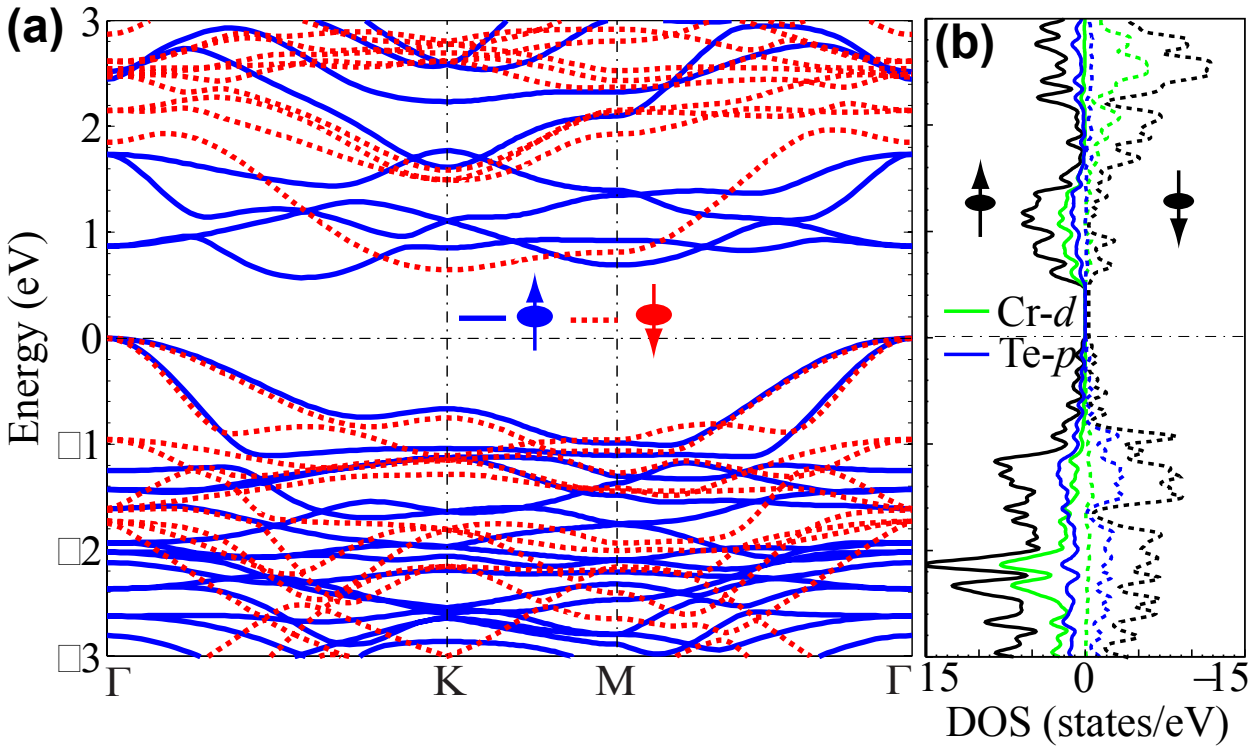

Figure 5. Electronic band structure obtained from first-principles calculations using density-functional theory (DFT). (a) The electronic band structures of spin-up and spin-down is denoted as blue and red. (b) Spin density of states show the bandgap of monolayer of $CiSiTe_3$ with the gap size 0.57 eV and 0.65 eV for spin up and spin down, respectively.

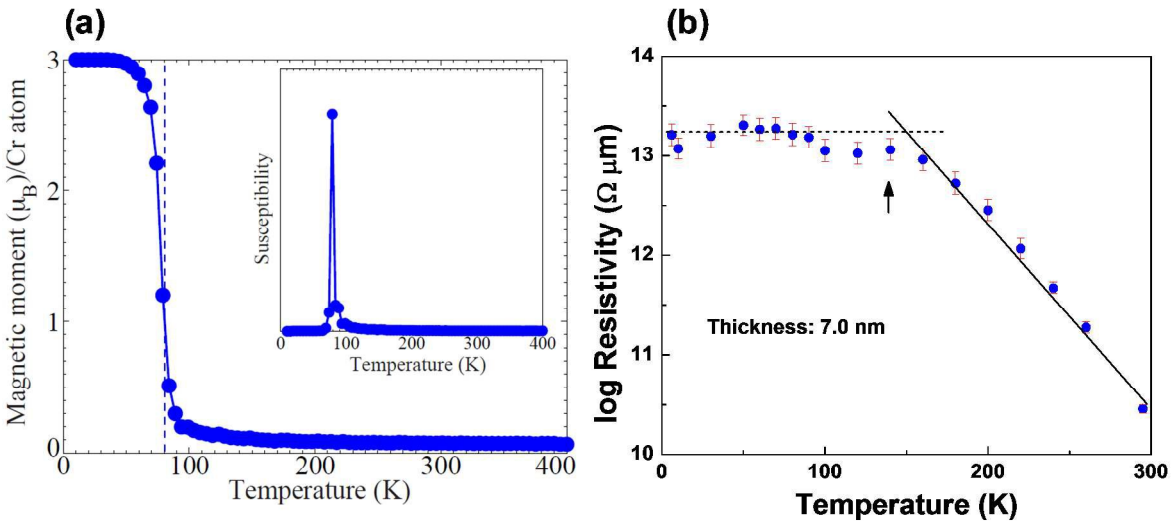

Figure 6. (a) The calculated transition temperature (T_c) with magnetic moment $3\mu_B$ for monolayer $CrSiTe_3$ using 2D Ising model Monte Carlo simulations with the exchange parameter from the LDA+U calculations. Inset shows the susceptibility as function of temperature for monolayer $CrSiTe_3$. (b) The plot of logarithmic resistivity vs. temperature for $CrSiTe_3$ flake of 7 nm thickness, exhibiting an expected increase in resisitivity with decreasing temperature in the high temperature regime, but with a clear deviation from this behavior beginning ~140K, indicating a possible FM-AFM phase transition at that temperature. Dashed line indicates the average resistivity for measurements T < 100K.

Table 1. Comparison between ferromagnetic (FM) and antiferromagnetic (AFM) structure (lattice constant a_0), magnetic moment μ_B, and formation energy E_f for monolayer $CrSiTe_3$.

	a_0 (Å)	μ (μ_B)	E_f
FM	6.69	3.0	43.7
AFM	6.66	3.0	48.7

TOC figure